PTV STUDY OF TURBULENT FLOW SEPARATION INDUCED BY A FORWARD-FACING STEP: A LAGRANGIAN PERSPECTIVE

Xingjun Fang
Institute of Mechanics
Chinese Academy of Sciences
Beiing, 100190, People's Republic of China
fangxj@imech.ac.cn

Seyed Sobhan Aleyasin
Department of Mechanical Engineering
University of Manitoba
Winnipeg, MB R3T 5V6, Canada
aleyasss@myumanitoba.ca

Sedem Kumahor
Department of Mechanical Engineering
University of Manitoba
Winnipeg, MB R3T 5V6, Canada
kumahors@myumanitoba.ca

Ebenezer Ekow Essel
Department of Mechanical, Industrial and
Aerospace Engineering,
Concordia University
Montreal, H3G 1M8, Canada
ebenezer.essel@concordia.ca

Mark F. Tachie
Department of Mechanical Engineering
University of Manitoba
Winnipeg, MB R3T 5V6, Canada
mark.tachie@umanitoba.ca

ABSTRACT

Turbulent separations induced by a forward-facing step (FFS) submerged in a thick turbulent boundary layer (TBL) were experimentally studied using a time-resolved particle tracking velocimetry. The Reynolds number based on the free-stream velocity and step height was 13 200. The oncoming TBL was developed over a cube-roughened wall, and the boundary layer thickness was 6.5 times the step height. Consequently, the FFS was exposed to excessively strong mean shear, turbulence intensity and large-scale motion in the oncoming TBL. The complete set of non-zero Reynolds stresses and triple velocity correlations are reported for turbulent flows over FFS. The topology of the in-plane Reynolds stresses exhibit dual local peaks: one upstream of the step and the other over the step. Strong spanwise fluctuating velocity occurs near the windward face of the step due to the interaction of oncoming TBL with the step. This research provides a novel Lagrangian perspective of the coherent structures induced by an FFS to supplement the Eulerian approach used in our previous research (Fang & Tachie, 2020; Fang *et al.*, 2021*b*).

1 Introduction

Flow separations induced by sharp-edged bluff bodies are of great importance to a broad range of engineering and environmental applications. A forward-facing step (FFS) is a canonical test geometry that has been routinely used to investigate the generic features of flow separations. Earlier works (e.g., Hattori & Nagano (2010), Sherry *et al.* (2010) and Essel *et al.* (2015)) primarily focused on the effects of varying boundary layer thicknesses, upstream wall roughnesses and Reynolds numbers on the statistical and structural characteristics of turbulent separating flows induced by FFS. More recent investigations (e.g., Pearson *et al.* (2013), Graziani *et al.* (2018) and Fang & Tachie (2020)) have been devoted to understanding the unsteady characteristics and mechanisms of flow separations, which reflect the dominant coherent structures and also possesses a direct relevance to flow-structure-interaction applications. It is now clear that the evolution of large-scale motions and hairpin structures embedded in the incoming turbulent boundary layer upstream of the FFS determine the unsteadiness and mutual interaction of separation bubbles upstream of and over the FFS.

Stüer *et al.* (1999) conducted the first ever particle-tracking measurement of separating flows induced by FFS at low Reynolds numbers. They reported a persistent three-dimensional (3D) topology of particle trajectories, featuring an open-type separating bubble upstream of the step and a Taylor-Görtler-like vortex over the step. The persistence of this 3D topology was later reiterated by Wilhelm *et al.* (2003) using direct numerical simulation (DNS) of separating flows induced by FFS with different configurations of incoming semi-random perturbation. Fang *et al.* (2021*b*) performed DNS for separating flows induced by an FFS with upstream fully developed turbulent channel flow and observed that oncoming hairpin structure interacts with the step to generate 3D streamlines similar to those observed by Stüer *et al.* (1999) and Wilhelm *et al.* (2003). In spite of previous experimental (Persoons *et al.*, 2006; Fang & Tachie, 2020) and numerical (Fang *et al.*, 2021*b*) studies, a complete set of non-zero second- and third-order moments of fluctuating velocity statistics and the associated 3D flow topology for separating flows induced by FFS at

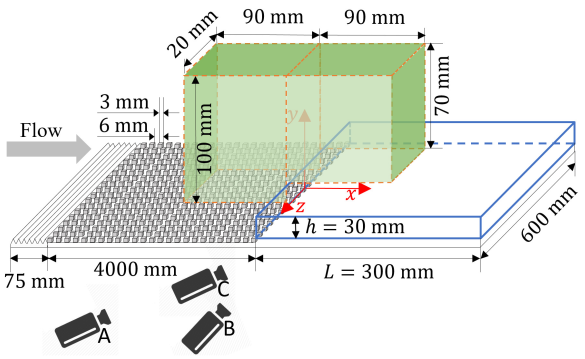

Figure 1. Schematic of the test geometry, adopted coordinate system as well as the measurement volume (green shaded volume) and camera configuration.

high Reynolds numbers remain unknown to date. Therefore, the present study experimentally investigates the statistical and structural characteristics of turbulent separations induced by an FFS submerged in a thick TBL using particle tracking velocimetry (PTV).

2 Experimental set-up

The experiments were conducted in an open recirculating water channel located in the Turbulence and Hydraulic Engineering Laboratory (THEL) at the University of Manitoba. Figure 1 shows the schematic of test geometry and camera configuration. To generate a thick TBL upstream of the FFS, turbulence transition was triggered at the entrance of the test section using toothed barriers, and the subsequent development of TBL was promoted by cube roughness on the bottom wall. The cube roughness elements were of side length 3 mm and pitch 6 mm in both the streamwise and spanwise directions. A step was mounted on the bottom wall immediately downstream of the rough wall. The streamwise length, vertical height (h) and spanwise width of the step were 300 mm, 30 mm and 600 mm, respectively. In the oncoming TBL, the free-stream velocity (U_∞) was 0.44 m/s, and the boundary layer thickness was 195 mm. The examined flow condition was identical to that in Fang & Tachie (2020) based on the planar PIV measurement. The values of Reynolds number based on free-stream velocity and step height was 13 200, and the boundary layer thickness was 6.5 times the step height. The turbulent intensity at the step height in the upstream turbulent boundary layer was 14.5%.

The water flow was seeded with 60 μm polyamide spheres. The flow field was illuminated using a diode pumped dual-cavity dual-head high speed Neodymium-doped yttrium lithium fluoride (Nd:YLF) laser. Three high speed 12-bit complementary metal oxide semiconductor cameras were arranged in the configuration of ⅃ (see figure 1). The cameras recorded the particle images at a resolution of 2560 pixel $\times$ 1600 pixel and a frame rate of 807 Hz. By using a commercial software (DaVis version 10) supplied by LaVision Inc., the Lagrangian velocities of seeding particles within the measurement volume (see figure 1) were calculated and subsequently post-processed using a set of in-house MATLAB® scripts.

Turbulent statistics were calculated directly using the Lagrangian data with the binning approach, and the side length of each bin is 1.08 mm. A few snapshots of Eulerian data were obtained by converting Lagrangian data to grids using the shake-the-box technique to qualitatively examine space-filled 3D vortical structures. The instantaneous velocities along the x, y and z directions are denoted by u, v and w, respectively, and the fluctuating component and ensemble averaging operation are denoted by superscript $(\cdot)'$ and over bar $\overline{(\cdot)}$, respectively.

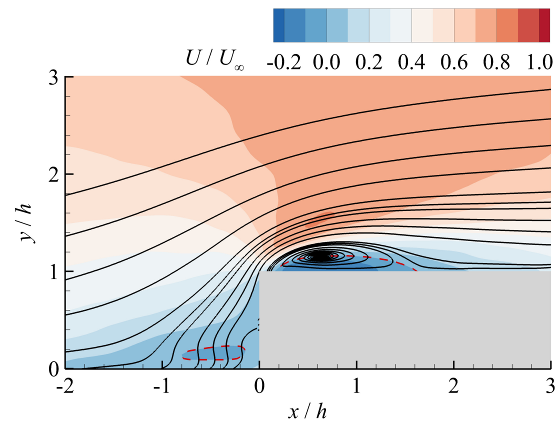

Figure 2. Contour of the streamwise mean velocity (U) superimposed with representative mean streamlines. The dashed isoplethes encompass the areas of flow reversal.

3 Results and discussion

Figure 2 examines the mean flow field from the present PTV measurement. Compared with that from the planar PIV measurement by Fang & Tachie (2020), the accuracy of mean flow field is reasonable except for the near-wall region upstream of the step. The mean flow is expected to detach from the bottom wall at $x/h \approx -0.9$, resulting in a distinct area of flow reversal immediately adjacent to the bottom wall upstream of the step. As seen in figure 2 upstream of the step, the exact detaching point is indiscernible and the reverse flow area deviates from the bottom wall. This disparity in comparison to the PIV results is attributed to the loss of particle tracks in the valleys of roughness element array. Indeed, over the step where no roughness elements existed, the mean reattachment length is identical to that (1.6h) reported in Fang & Tachie (2020).

Figure 3 plots the contours of all non-trivial Reynolds stresses $\overline{u'u'}$, $\overline{v'v'}$, $\overline{u'v'}$ and $\overline{w'w'}$. From the figure, $\overline{u'u'}$, $\overline{v'v'}$ and $\overline{u'v'}$ all possess dual local peaks: one upstream of the step and the other over the step. The magnitudes of the upstream and downstream peaks of $\overline{v'v'}$ are comparable, and so are those of $\overline{u'v'}$. These observations are in good agreement with those observed by Fang & Tachie (2020). The local peaks of Reynolds stresses upstream of the step signifies the interaction of incoming TBL with the step. Indeed, as concluded by Wilhelm *et al.* (2003), the transition to turbulence initiates in the rear part of the separation bubble over the step without incoming turbulence. As shown in Graziani *et al.* (2018), when the thickness of incoming turbulent boundary layer is smaller than the step height, the local peaks of $\overline{v'v'}$ and $\overline{u'v'}$ upstream of the step still manifest, but their peak values become apparently lower than those over the step. It is interesting to see in figure 3(d) that $\overline{w'w'}$ peaks upstream of the leading edge of the step. In fact, in the region close to the windward face of the step, the magnitudes of $\overline{w'w'}$ are evidently larger than $\overline{u'u'}$ and $\overline{v'v'}$. The same observation was also made by in the DNS study by Fang *et al.* (2021*b*), which was performed at a decade-lower Reynolds number. Fang *et al.* (2021*b*) attributed the significant levels of $\overline{w'w'}$ to the interaction of incoming hairpin structure with the step. More specifically, the principal stretching immediately upstream of the step is in the vertical direction, so that

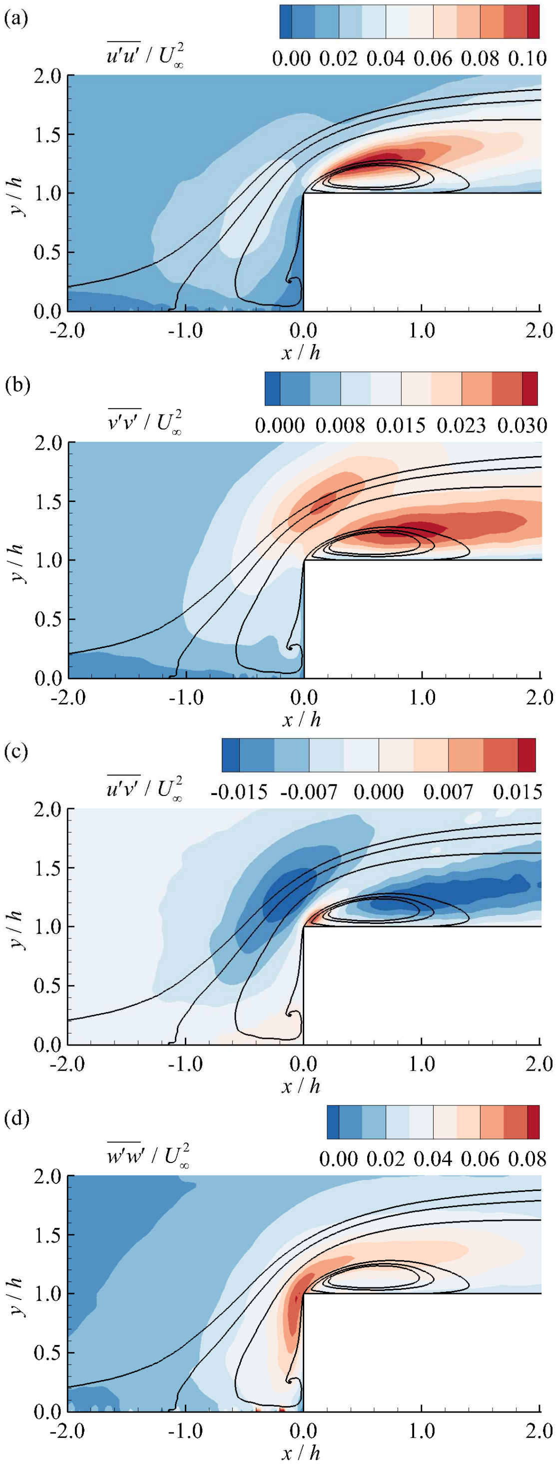

Figure 3. Contours of Reynolds stresses (a) $\overline{u'u'}$, (b) $\overline{v'v'}$, (c) $\overline{u'v'}$ and (d) $\overline{w'w'}$ superimposed with representative mean streamlines.

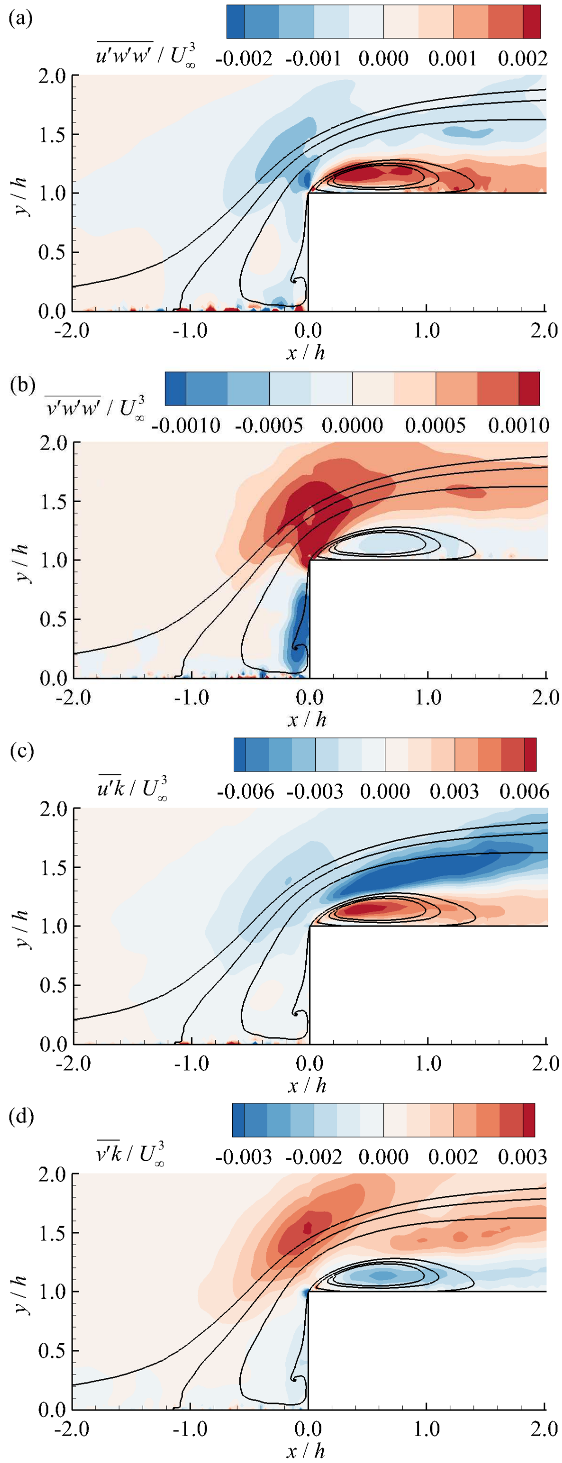

Figure 4. Contours of third-order moments (a) $\overline{u'w'w'}$, (b) $\overline{v'w'w'}$, (c) $\overline{u'k}$ and (d) $\overline{v'k}$ superimposed with mean streamlines, where $k = \frac{1}{2}(u'u' + v'v' + w'w')$ is the instantaneous turbulence kinetic energy so that $\overline{u'k} = \frac{1}{2}(\overline{u'u'u'} + \overline{u'v'v'} + \overline{u'w'w'})$ and $\overline{v'k} = \frac{1}{2}(\overline{u'u'v'} + \overline{v'v'v'} + \overline{v'w'w'})$.

the counter-rotating vortices (constituting hairpin legs) are deformed to attach onto the frontal surface of the step in the vertical direction. This mechanism thus generates elevated $\overline{w'w'}$ along the deformed hairpin legs mounting over the step.

Figure 4 shows all non-trivial third-order moments unavailable from planar PIV measurement. From the figure, $\overline{u'w'w'}$ and $\overline{v'w'w'}$ switch sign near the mean separating streamline over the step. This indicates that ejection (featuring $u' < 0$ and $v' > 0$) and sweep (featuring $u' > 0$ and $v' < 0$) events are dominant, respectively, in the regions upstream of and within the mean separation bubble over the step. This is consistent with the deduction from Fang *et al.* (2021*a*) at a much lower Reynolds number. Additionally, a distinct edge emanating from the leading edge manifests in the contours of all second- and third-order moments. This edge was also reported by Fang & Tachie (2020) and Fang *et al.* (2021*b*), as a 'shield' demarcating different interaction mechanisms of the coherent structures embedded in the incoming TBL with

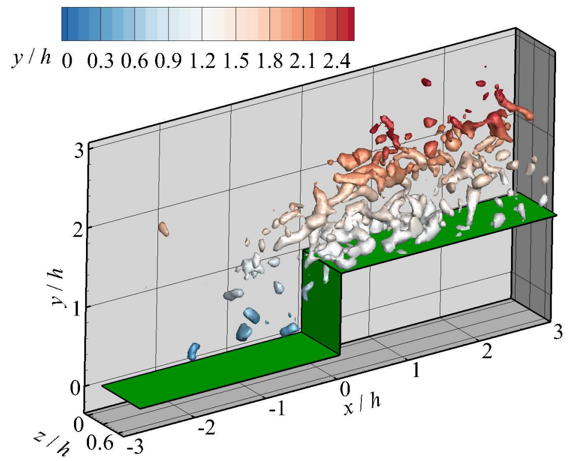

Figure 5. Isosurface of $\lambda_{ci} = 2.6U_\infty/h$ in a typical instantaneous flow field.

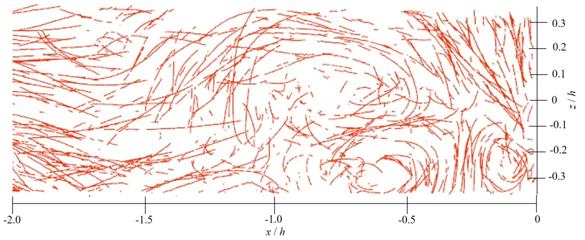

Figure 6. Projections of representative particle trajectories onto the x-z plane for $y/h \in [0.6, 1.0]$.

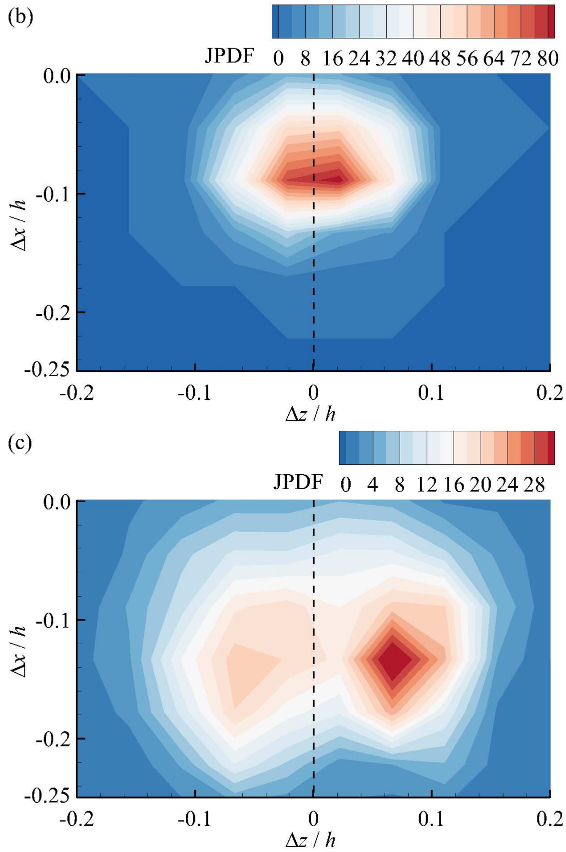

Figure 7. Joint probability density function (JPDF) of particle displacement relative to particles within $x/h \times y/h \in [-0.39, -0.13] \times [0.87, 1.13]$ at Δt time apart: (a) $\Delta t = -0.11h/U_h$ and (b) $\Delta t = -0.22h/U_h$.

step. Upstream of this 'shield', the ejection event is dominant immediately upstream of the leading edge. This is because the principal stretching is nearly along the mean streamline so that vortices tend to be align with the mean streamline in the vicinity. The dominance of ejection event further suggests that the aforementioned vortices along mean streamlines come in pairs, so that the fluid flanked by the vortex pair immediately upstream of the leading edge is significantly pumped backwards and upwards to generate ejection event. This mechanism is strong especially considering the acute curvature of vortices imposed by the leading edge.

Instantaneous vortical structures are visualized in figure 5 using the isosurface of λ_{ci}, which identifies a vortex in the region of positive λ_{ci} (Zhou *et al.*, 1999). From the figure, the density of identified vortices increases abruptly as the step is approached. This is similar to the observation in Fang *et al.* (2021*b*) and is attributed to the generation of strong vortical structures through interaction of incoming turbulence with the separating flows. More specifically, the vortical structures are not confined within the shear layer emanating from the leading edge, and there is no trace of spanwise vortices in the separated shear layer as those in transitional separating flows (e.g., Cimarelli *et al.* (2018)). These suggest the profound disruption of vortical structures by the incoming turbulence. In fact, vortex tubes leaning over the leading edge of the step are evident from the figure, while the vortex tubes over the step tend to be streamwise orientated. These observations generally agree with the pattern of vortical structures resulting from interaction of incoming hairpin structure with the step (Fang *et al.*, 2021*b*).

To further examine the flow structure upstream of the step, figure 7(a) provides a top view of some representative particle trajectories. As the step is approached, particle trajectories develop into swirling patterns,while inducing spanwise motion near the frontal surface of the step. This agrees with the strong $\overline{w'w'}$ upstream of the step shown in figure 3(b). Some of the particle trajectories in figure 7 are reminiscent of counter-rotating vortices. This is similar to the conclusion by Fang & Tachie (2019) that as the step is approached, the spanwise-alternating-signed streaky structures embedded in the incoming turbulent boundary layer become narrower and a pair of counter-rotating vortices occur immediately upstream of windward face of the step.

To further explore the aforementioned deduction of strong variation of vortical structures immediately upstream of the leading edge, all particle entering a box ($x/h \times y/h \in [-0.39, -0.13] \times [0.87, 1.13]$) is tagged. The probability of x and z coordinates of these tagged particles before entering this box is examined in figure 7, so as to statistically examine the trajectories of particles passing over the step near the leading edge. It is evident in figure 7 that at a larger time displacement, the x-z positions of the particles show bi-modal distribution. In other words, particles approaching the step tend to deviate from its original spanwise plane as passing over the step. This is reminiscent of the open-type separation bubble upstream of the step noted by Stüer *et al.* (1999), as well as the counter-rotating vertical vortices upstream of the step observed by Fang *et al.* (2021*b*). Since the hairpin structures are effective in terms of generating out-of-phase interaction between the separation bubbles upstream of and over the step, even at high Reynolds numbers (Fang & Tachie, 2020). It is reasonable to deduce that the bi-modal JPDF in figure 7(b) is attributed to the vertical counter-rotating vortices through the same stretching mechanisms elucidated by Fang *et al.* (2021*b*).

4 Conclusions

Turbulent separating flows induced by a forward-facing step (FFS) immersed in a deep turbulent boundary layer is studied using particle tracking velocimetry (PTV). The Reynolds number based on free-stream velocity and step height is 13 200. The PTV measurement gives access to the three velocity components of particles within a measurement volume possessing a spanwise thickness of 2/3 step height. PTV could easily lose track of those particles that go in and out of the space between roughness elements, but generates decant measurement accuracy overall compared with the planar particle image velocimetry (PIV). The obtained Lagrangian data is particularly valuable in terms of calculating all non-zero turbulent statistics and exploring the three-dimensional (3D) characteristics of vortical structures.

The results show that spanwise Reynolds normal stress $\overline{w'w'}$ peaks in an area immediately adjacent to the windward face of the step, and its peak value is significantly stronger than other Reynolds normal stresses in the same location. The third-order moments further indicate that the ejection event is dominant immediately upstream of the step. The overall structural mechanism is as follows. The streamwise elongated streaky structures residing in the upstream turbulent boundary layer becomes narrower and amplified as approaching the step, and eventually, a pair of the counter-rotating vortices manifest in the streamwise-spanwise plane immediately upstream of the step. This pair of vortices extend upwards and become aligned with the mean streamline immediately upstream of the leading edge. Near this location, this pair of vortices is abruptly bent by the leading edge corner, and the resulted acute curvature of vortices significantly enhanced the pump-up of fluid in the area flanked by the vortices. This generates excessive ejection event immediately upstream of the step. This ejection event is switched to sweep event abruptly over the step along the separated shear layer. This sweep event is elongated in the streamwise direction, consistent with the Taylor-Görtler-like vortex over the step reported by Stüer *et al.* (1999) albeit at much lower Reynolds number.

Acknowledgements

The financial support from Natural Sciences and Engineering Research Council (NSERC) of Canada and Canada Foundation for Innovation (CFI) to M.F.T. is gratefully acknowledged.

REFERENCES

Cimarelli, A., Leonforte, A. & De Angeli, E. 2018 On the structure of the self-sustaining cycle in separating and reattaching flows. *J. Fluid Mech.* **857**, 907–936.

Essel, E. E., Nematollahi, A., Thacher, E. W. & Tachie, M. F. 2015 Effects of upstream roughness and Reynolds number on separated and reattached turbulent flow. *J. Turbul.* **16(9)**, 872–899.

Fang, X. & Tachie, M. F. 2019 On the unsteady characteristics of turbulent separations over a forward-backward-facing step. *J. Fluid Mech.* **863**, 994–1030.

Fang, X. & Tachie, M. F. 2020 Spatio-temporal dynamics of flow separation induced by a forward-facing step submerged in a thick turbulent boundary layer. *J. Fluid Mech.* **892**, A40.

Fang, X., Tachie, M. F. & Bergstrom, Donald J. 2021*a* Direct numerical simulation of turbulent flow separation induced by a forward-facing step. *Intl J. Heat Fluid Flow* **87**, 108753.

Fang, X., Tachie, M. F., Bergstrom, D. J., Yang, Z. & Wang, B. 2021*b* Three-dimensional structural characteristics of flow separation induced by a forward-facing step in a turbulent channel flow. *Journal of Fluid Mechanics* **919**, A24.

Graziani, A., Kerhervé, F., Martinuzzi, R. J. & Keirsbulck, L. 2018 Dynamics of the recirculating areas of a forward-facing step. *Exper. Fluids* **59**, 154.

Hattori, H. & Nagano, Y. 2010 Investigation of turbulent boundary layer over forward-facing step via direct numerical simulation. *Intl J. Heat Fluid Flow* **31(3)**, 284–294.

Pearson, D. S., Goulart, P. J. & Ganapathisubramani, B. 2013 Turbulent separation upstream of a forward-facing step. *J. Fluid Mech.* **724**, 284–304.

Persoons, T., Hoefnagels, A. & den Bulck, E. Van 2006 Calibration of an oscillating hot-wire anemometer for bidirectional velocity measurements. *Exper. Fluids* **40**, 555–567.

Sherry, M., Lo Jacono, D. & Sheridan, J. 2010 An experimental investigation of the recirculation zone formed downstream of a forward facing step. *J. Wind Eng. Ind. Aerodyn.* **98(12)**, 888–894.

Stüer, H., Gyr, A. & Kinzelbach, W. 1999 Laminar separation on a forward facing step. *Eur. J. Mech. B/Fluids* **18**, 675–692.

Wilhelm, D., Härtel, C. & Kleiser, L. 2003 Computational analysis of the two-dimensional-three-dimensional transition in forward-facing step flow. *J. Fluid Mech.* **489**, 1–27.

Zhou, J., Adrian, R. J., Balachandar, S. & Kendall, T. M. 1999 Mechanisms for generating coherent packets of hairpin vortices in channel flow. *J. Fluid Mech.* **387**, 353–396.